UNIVERSITY OF CALIFORNIA, SAN DIEGO

BDNF IMBALANCE IN MECP2-DEFICIENT MICE MAY BE LINKED TO AXONAL TRANSPORT DEFECTS

A thesis submitted in partial satisfaction of the requirements for the degree Master of Science

in

Biology

by

Po Han Lin

Committee in charge:

Professor Chengbiao Wu, Chair
Professor Stefan Leutgeb, Co-Chair
Professor Jill Leutgeb

2014

The thesis of Po Han Lin is approved, and it is acceptable in quality and form for publication on microfilm and electronically:

_____

_____

Co-Chair

_____

Chair

University of California, San Diego

2014

DEDICATION

I dedicate this thesis to Dr.Pavel Belichenko, Mom, Dad, and Homie, for their love and support.

TABLE OF CONTENTS

LIST OF FIGURES

LIST OF TABLES

ACKNOWLEDGEMENTS

I would like to first express my thanks for Dr.Pavel Belichenko for bringing me into the lab and giving me an opportunity to engage in both the joy and pain that is research. Although he is no longer with us, his amiable personality and dedication to science is something that I would always carry with me.

I would also like to give my tremendous appreciation for Dr.Chengbiao Wu, for his support after the passing of Dr.Belichenko and agreeing to sponsor me as the co-chair of my committee. His team of wonderful researchers, April Weissmiller, Xiaobei Zhao, Pauline Hu, and many others, all played crucial roles in providing guidance during my journey through this project.

The Results chapter, in part, is currently being prepared for submission for publication of the material. Lin, Po Han. Hu, Yue. The thesis author was the primary investigator and co- author of this material.

ABSTRACT OF THE THESIS

BDNF IMBALANCE IN MECP2-DEFICIENT MICE MAY BE LINKED TO AXONAL TRANSPORT DEFECTS

by

Po Han Lin

Master of Science in Biology

University of California, San Diego 2014

Professor Chengbiao Wu, Chair

Professor Stefan Leutgeb, Co-Chair

Rett syndrome (RTT), a rare neurodevelopmental disease found in 1:15,000 of female births, is an autism spectrum disorder involving mutations of the MeCP2 gene on the X-chromosome in human. In recent years, researchers have investigated and

found evidence of the correlation between abnormal distribution of brain-derived neurotrophic factor (BDNF) and the pathology of RTT. However, few have explored the mechanism behind the regional shortage of BDNF in the brain. Here, I demonstrate that MeCP2-deficiency in MeCP2B cortical neurons, a mice model of RTT, is associated with impaired axonal transport of BDNF. In addition, I also established evidence suggesting that lithium treatment of neurons enhances axonal transport of BDNF in a p-Tau-dependent manner. Together, these findings provide a step forward in understanding the neurological background of the disease, and suggest a hypothetical model of the mechanism behind MeCP2-deficiency and neuronal BDNF imbalance.

INTRODUCTION

Rett Syndrome

A postnatal neurodevelopmental disorder, Rett syndrome (RTT) was first discovered in 1954 when an Austrian physician, Dr. Andreas Rett, came across multiple girls exhibiting the same repetitive hand wringing behaviors while in his clinic. Although he later characterized the symptoms in his article in 1966, the disorder did not catch wide attention of the medical community until 1983, when Swedish researcher Dr. Bengt Hagberg also published his findings in a more mainstream English journal, Annals of Neurology. (ref. 1-2) Since then, RTT has undergone significant scientific investigation, and is most recently categorized in the Diagnostic and Statistical Manual of Mental Disorders, 4th Edition, Text Revision (DSM-IV-TR) as a type of pervasive developmental disorder. (ref. 3) A genetically inherited disease stemming from the mutations of the methyl CpG binding protein 2 (MeCP2) gene on the X-chromosome, RTT affects mainly the female population with occasional male patients having been documented in the past. RTT is considered to be a rare neurological condition due to its low occurrence frequency of approximately 1 in 15,000 female births.

While symptoms such as motor and speech dysfunctions, decreased head growth, and motions of hand wringing are classic characterizations of RTT, the manifestation of these symptoms occurs through four stages of the disorder: (ref. 4-5)

Stage 1 – Early onset stage

- First 6-18 months of age
- Females are usually normal or with vague symptoms
- Delays in motor ability, speech, and autistic-like symptoms such as reduced eye contact and social interactions occur slowly but often not noticeable

Stage 2 – Rapid destructive stage

- Occurs during age 1 to 4, usually for weeks to months
- Significant loss of purposeful motor movement and the ability to walk steadily
- Characteristic hand movement such as wringing, clapping, and repeatedly moving hand to mouth begin to manifest at this stage
- Autistic-like symptoms can also appear
- Noticeable loss of verbal skills and slowed head growth
- Some of the symptoms may improve or even disappear during sleep

Stage 3 – Plateau/pseudo stationary stage

- Occurs during age 2 to 10 and lasts for years
- Patients can continue to exhibit symptoms of apraxia and motor disabilities

- Seizures can become a problematic occurrence (ref. 6)
- Social behaviors and autistic-like features related to attention span and alertness may show improvement
- Many remain in this stage for the most of their lives

Stage 4 – Late motor deterioration stage

- May last years to decades
- Prominent features include further reduced motility with muscle weakness and rigidity
- Scoliosis and spasticity are common
- Cognitive function and hand skills generally stopped declining at this stage

At the moment, diagnosis of RTT relies mainly on the clinical observation of early developmental signs, especially during the rapid destructive stage of the disorder, and genetic testing to identify mutations on the MECP2 gene. Unfortunately, there is currently no cure for RTT. Treatments focus on alleviating and managing the symptoms, and medications are commonly prescribed for breathing irregularities and motor difficulties. Occasionally, anticonvulsant drug may also be necessary for controlling seizures. In the later stages of the disorder, frequent monitoring for scoliosis is also recommended. While no cure is yet available, through careful

management of symptoms many individuals with RTT continue to live well into middle ages or beyond. Nevertheless, due to the rarity of the disease, no reliable estimate for life expectancy beyond the age of 40 has been established.

Methyl CpG Binding Protein 2

Methyl-CpG binding protein 2 (MeCP2), a member of the nuclear protein family methyl binding domains (MBD), has been conventionally viewed as a universal transcriptional repressor that binds with high affinity to methylated DNA at CpG sites. (ref. 7) Consisted of 486 amino acids and weighting approximately 53 kDa, MeCP2 has been well characterized for its wedge-like methyl-CpG binding domain and its transcriptional repression domain (TRD) (ref. 8). The methyl binding domain is an 85 amino acid region responsible for the specific binding of MeCP2 to cytosines on CpG sites, which are commonly found near the promoter region of genes and are largely methylated. Evidence suggests this behavior to occur both in vitro and in vivo, as chromatin immunoprecipitations (ChIP) of mice had exhibited uneven localizations of MeCP2 which concentrate on the CpG-rich heterochromatins (ref. 9). In the event of deletion or mutation to key amino acids in this region, the selectivity and silencing ability of MeCP2 also become significantly impaired (ref. 8).

The TRD, on the other hand, is a 105 amino acids region that comprises the core of the protein's repressive mechanism. By recruiting corepressor mSin3A and histone deacetylases (HDACs) to form repressor complexes, the TRD is essential for the transcriptional repression of MeCP2 by compacting chromatin structure through

inhibitory modifications such as histone deacetylation and methylation (ref. 10-11). Moreover, recent publications have demonstrated evidence of MeCP2 inducing repression through association with histone methyl-transferase and introducing methylation to chromatins (ref. 12).

In essence, previous investigations have established a model ofMeCP2 as a universal protein which represses transcriptional activity of genes through interactions with methylated CpG sites near promoters, and recruiting corepressor mSin3A and HDACs to alter chromatin structure to inhibit access to transcription. However, subsequent studies have suggested that MeCP2 may have multiple mechanics of transcriptional silencing beyond the scope of the conventional model.

An alternative model has proposed a different mechanism of how MeCP2 may repress transcription through HDAC-independent interaction to achieve chromatin compaction. When highly purified MeCP2 were presented to nucleosome at molar ratios of approximately 1.0 MeCP2/nucleosome, an elliptoid architecture of compacted chromatins was observed through electron microscopy (EM) (ref. 13). As nuclease digestion was imposed to investigate the nature of this compaction, degradation of the linker DNA but not the chromatin suggests that MeCP2 interacts with chromatins directly and was able to stabilize the compacted nucleosomal array, while the linker DNA between nucleosomes was not involved in this process and was digested. Moreover, when the experiment is repeated with a mutated MeCP2 which the MBD is dysfunctional, the same elliptoid formation of chromatin compaction was

not interfered. This suggests that MeCP2 may be able to modify the architecture of chromatins independent of interaction with methylated DNA. The 1-to-1 molar ratio of MeCP2 protein and nucleosome which is required for this to occur is also strongly indicative of specific interactions between individual MeCP2 molecules and nucleosome. (ref. 14)

In addition to the structural model of MeCP2-induced chromatin modification that is independent of methylated DNA binding, MeCP2 has further been found to play a role in RNA splicing regulation (ref. 15) and silent chromatin looping (ref. 16). One recent finding that poses perhaps the biggest challenge for the conventional model of methyl-dependent MeCP2 silencing is the discovery of low percentage of MeCP2 binding to methylated promoter regions during an epigenomic analysis (ref. 17). Using a custom designed oligonucleotide microarray consisted of known or potential target genes of MeCP2, ChIP analysis revealed that 59% of MeCP2 binding sites are beyond gene boundaries, and only 6% of MeCP2 bindings are near promoter regions. Among those 6%, majority of the promoters belonged to active genes, which is inconsistent with the conventional model suggesting that MeCP2 occupancy at promoters brings silencing of the genes. Moreover, the analysis further indicated that the majority of highly methylated promoters are not bound by MeCP2 proteins. These discoveries support the structural model as MeCP2 largely behaves independent of methylated DNA, and suggests evolved roles of MeCP2 from the classic model as epigenetic silencer.

Today, the functions of MeCP2 are predicted to be related to transcriptional silencing and activation, along with chromatin compaction and remodeling. In order to further elucidate the mechanisms of how MeCP2 influences transcriptional activities, higher resolution of DNA mapping for methylation sites for comparison with ChIP analysis may be needed (ref. 18)

While a comprehensive model for the precise molecular interactions of MeCP2 has yet been developed, much has been learned about the effect of its universal expression, especially its importance in the development of central nervous systems. (ref. 19) When Dr. Huda Zogbhi published her findings of RTT as a X-linked genetic disorder in 1999, she was the first among many to establish mutations on the MECP2 gene as the cause for RTT. (ref. 20) Since then, other researchers have further produced lines of evidence supporting this relationship between the inheritance of MECP2 mutations and RTT (ref. 21-27), and the rare instances where the condition was documented to arise from sporadic mutations (ref. 28).

These mutations on MeCP2 have been noted to cause severe cognitive, motor, and autonomic dysfunction in both mice and human (ref. 29) In fact, as a range of autistic-like behaviors are classic features of RTT, affected patients are considered as a part of the autism spectrum disorder population (ASD). In the past, studies performed on the brains of subjects with RTT and on mouse models of RTT have shown that the Mecp2 mutation has relatively little influence on neurogenesis and neuronal migration.

The organization of cortical layers and the structure of the hippocampus are largely unaffected (ref. 30-34).

In contrast, striking changes in neuronal circuit structure have been documented. Most striking are changes in the structure of dendrites and in the spines that decorate dendrites. It is noteworthy that dendritic spines signal the locus of synapses.The changes detected included: 1) significant reductions in the number and length of dendrites; 2) decreased dendritic spine number and regional loss of spines in the cortex; and 3) disorganization of afferent fibers to the spines of pyramidal neurons and in the shape of the axonal bundles in which they travel (ref. 35-36, 8). The evidence is thus consistent that RTT exerts pathogenetic events that impact the maturation of neurons and the circuits in which they participate (ref. 8, 34, 37-38).

Recently, the brain anatomy, dendritic and axonal phenotypes in two mouse models of RTT (Mecp2B and Mecp2J mice) have been established to compare the size, shape and volume of a number of brain regions, along with dendritic and axonal morphology between male mutant and WT littermates (ref. 34, 38). It was concluded that the pathogenesis of RTT implicates numerous brain regions and axonal connections. Coupled by numerous experimental data revealing significant relationships between MeCP2 deficiency and alterations in growth factors (ref. 39-45), it becomes of importance to investigate whether MeCP2 plays a critical role in altering the synthesis, transport, and signaling of neuronal growth factors such as brain-derived

neurotrophic factors (BDNF), thereby causing dysregulation of neuronal circuit structure development and function when MeCP2 becomes deficient in RTT patients.

Brain-derived neurotrophic factor

Brain-derived neurotrophic factor (BDNF) is a neurotrophin produced from one of the target genes of MeCP2, BDNF, which plays a crucial role in the structure development of neuronal circuitry. Moreover, it has been reported to also play a role in the survival of neurons, memory formation, the development and differentiation of immature neurons, synaptic plasticity, and neuronal connectivity throughout life (ref. 46-49)

A gene with its transcriptional activity dependent on the level of neuronal activity, BDNF is also regulated by the repressive transcriptional protein MeCP2. It was originally predicted that with the deficit of functional MeCP2, the expression of BDNF should rise with the same level of neuronal activity in RTT subjects. However, the level of BDNF was observed to be markedly reduced in the absence of functional MeCP2 (ref. 39). In a whole brain lysate analysis, only about 70% of level of BDNF protein present in wild-type mice was present in RTT mutant mice (ref. 41). As recent studies have documented the correlations between these abnormalities in BDNF expression with aforementioned phenotypic changes such as reduced cerebral size and structural abnormality in the brainstem, they provide a direction for investigating the molecular basis behind RTT symptoms through examining the expression of BDNF.

Since then, significant progress has been made in normalization of BDNF level resulting therapeutic effect on some phenotypes in mouse models of RTT (ref. 41, 43, 50-52). While these findings suggests plasticity in the BDNF expression of RTT subjects, the precise mechanism behind how BDNF levels influence changes in spine and axonal morphology is still unclear. One hypothesis of how growth factors affect the neuronal connections has been propose to question the mechanism behind the matching of synaptic connections, which is necessary for efficient circuit function and development.

During pre- and postnatal development specific neuronal circuits are established in each brain region to integrate and process incoming information. The growth of axons to their target neurons and the creation of appropriately matched synapses at those sites are necessary for robust and proper communication between the neurons. As neurons communicate with each other via synapses made between axons and cell body and dendrites, the releasing of neurotrophic factors for neurons to signal information such as size, activity status and type is crucial for proper matching of synapses and appropriate development of neuronal circuits. As data has shown that these matching processes are severely altered on both mouse models of RTT and on subjects with RTT (ref. 32, 34, 37-38), the results point toward a possible flaw in the transport of neurotrophic factors in RTT patients. Interestingly, the defect in axonal transport of BDNF was shown recently in rat cortical neurons transfected with Mecp2 siRNA (ref. 53). When inhibited by the siRNA, MeCP2 deficient rat neurons exhibit impaired transport velocities in both the retrograde and anterograde directions. The

finding was correlated with a reduction of Huntingtin (Htt) and huntingtin-associated protein (Hap1), proteins involved in the axonal transport of BDNF, in the brains of RTT mice. The researchers hypothesized that the mechanism is similarly impaired in the mice models of MeCP2, MeCP2B and MeCP2J, thereby causing the observed reduction of BDNF level in the striatum of MeCP2- mice, where the main source of BDNF is through axonal transport from the cortex.

While the discovery suggests a step forward in understanding the disorder, confirmation of the same axonal transport impair in mice models of RTT is needed to corroborate with the immunochemistry data, which were derived from mice instead of rats. Therefore, the major goal of this proposal is to determine whether MeCP2 dysfunction affects neurotrophic signals trafficking in neuronal networks containing MeCP2+ and MeCP2- cortical neurons from a mice model of RTT. We suspect that while normal expression of Mecp2 maintains adequate axonal transport of BDNF and proper pre- and postsynaptic contacts, when functional MeCP2 is deficient it may alter and impair characteristics of BDNF transport in MeCP2- neurons, thereby causing dysregulation of neuronal circuit structure and function.

RESULTS

Confirmation of phenotypic MeCP2 expression matching with different genotypes of MeCP2bird strain mice

I started this project by analyzing the presence of nuclear protein MeCP2 in neurons of various genotypes from the MeCP2bird mice model of RTT, seeking to establish a preliminary confirmation of the connection between MeCP2 expression and genotypes in this particular mice strain as basis for later experimentation. I plan to achieve this goal through immunostaining mass cultures of cortical neurons from MeCP2B litters, which by probability would contain wild-type mice, MeCP2+/- females, and MeCP2-/y males. Using the methodology that is routinely practiced in the lab and maintenance techniques found in previous publication (ref. 34), I cultured cortical neurons from these P0 MeCP2B litters on coated glass coverslips in 12-well dishes. The rationale of using P0 mice is both to save female mice for further pregnancy, and because RTT is a disorder with its symptoms mainly manifested in the postnatal stage. On DIV 7, the neurons are fixed with paraformaldehyde to retain structural integrity, and stained with both the antibody against MeCP2 to reveal MeCP2 expression and acridine orange for the tagging of neuronal cell bodies. The neurons are then examined under the confocal microscope for immunofluorescence, and then compared with their respective genotypes from genotyping.

Using this approach, I was able to establish that MeCP2 protein is present in all neurons from wild-type mice, interspersed in MeCP2+/- females, and completely

absent in neuronal cultures of MeCP2-/y males. (Figure 1.) This result affirms my initial expectations, as patterns of MeCP2 expression in cultures are found to match with the genotypes of the particular mice they are cultivated from. This provides a basis for me to pursue further experimentations using litters from this particular mice model of RTT.

Microfluidic chamber cultures revealed impairments in the axonal transport of BDNF in MeCP2-deficient mice neurons

Next, I explored the characteristics of axonal transport of BDNF in both wild-type and MeCP2- mice with a recently developed technique in the lab, using biologically active, monobiotinylated BDNF (mBtBDNF) that can be conjugated to Quantum-dot 655 (QD655) with streptavidin to study axonal transport using live imaging. As designed, one BDNF molecule is only labeled with one biotin; when conjugated to QD-655, the resulting BDNF-Quantum dot 655 (BDNF-QD655) emits fluorescence under live imaging microscope and can be used to track BDNF-containing vesicles and study axonal transport in cortical neurons in microfluidic chamber cultures.

Moreover, I adopted the technique of culturing neurons in microfluidic chambers for the aims of this experiment, which has been a standard for conducting live imaging of axonal transports in past articles (ref. 54-55). By using microfluidic chamber cultures in lieu of mass cultures in this experiment, I was able to create

fluidic isolations between the cell body and distal axons, optimizing BDNF uptake and facilitating the observations of axonal transport.

I cultured MeCP2B litters on postnatal day 0 (P0) to create microfluidic cortical neuronal cultures, and maintained the cultures with techniques similar to mass culture. During the interim, I genotyped mice tails to select cultures from MeCP2-/y males for experimentation and wild-type mice cultures as the control group. On DIV 7, both groups are starved of BDNF for 2 hours, and then fed with medium containing 25 mM BDNF-QD655 in the distal axon channels for an additional 2-4 hrs. Live imaging of the axonal transport of BDNF-QD655 within proximal axons is done in an environmentally-controlled setup, and recorded by a Leica microscope with a frame capturing speed of 1/sec. The time-lapse image series are then analyzed using kymographs produced from ImageJ (Figure 2A), noting the following parameters with respect to axonal transport of BDNF-QD655: 1) instantaneous velocity of both retrograde and anterograde transport; 2) frequency and duration of pausing between both retrograde and anterograde traffic. Stationary and mobile vesicles are distinguished in this step of the analysis, and only actively moving vesicles containing BDNF are analyzed (Figure 2B).

Analyzing dataset with two-tailed t-tests, I was able to determine marked impairments in the transport velocities of MeCP2-deficient mice neurons in both the retrograde (Mean ± SEM = 1.481±0.06094) and anterograde (Mean ± SEM = -0.6405±0.1080) directions when compared to wild-types (1.773±0.07762 and -

1.155±0.1454, respectively). (Figure 2C) While the decreases in retrograde (-16.5%) and anterograde (-44.5%) velocities are significant, the change in retrograde transport dynamic is less drastic than previously documented (ref. 53), which may be due to differences in the backgrounds between mice and rat samples, or differences between MeCP2 deficiencies caused by mutation versus siRNA silencing. Nevertheless, these results suggest the previously observed changes in the dynamics of BDNF transport in siRNA-silenced MeCP2-deficient rat could also occur in the MeCP2B mice model of RTT, pointing toward a high likelihood that MeCP2-deficiency influences mechanisms of BDNF transport in RTT subjects.

Enhancement of BDNF axonal transport through lithium chloride treatment

With the finding that reduced level of functional MeCP2 protein could negatively impact the axonal transport of BDNF, I moved on to investigate potential therapeutic treatments that could rescue the transport changes observed in MeCP2-deficient neurons. One treatment which I explored was the application of lithium chloride in neuronal cultures, which has been documented in the past to reduce phosphorylated Tau (p-Tau) in subjects with Alzheimer's disease through inhibiting glycogen synthase kinase-3 (GSK-3). (ref. 56)

The reduction of p-Tau level is of interest here as p-Tau has been noted to cause excessive depolymerization of microtubules, thereby interfering with neurite stability and causing defects in the axonal transport of neurotrophic factors. (ref. 57-58) As BDNF has also been implicated as a regulator of p-Tau levels both directly through

dephosophorylation (ref. 59) and indirectly through inhibition of GSK-3 and prevention of its kinase activity on Tau (ref. 60), the shortage of BDNF in the striatum may have an amplifying effect on its impaired transport due to an increased level of p-Tau (ref. 61). Therefore, by inhibiting GSK-3 with lithium and reducing the p-Tau level, we may be able to observe a rescuing effect on the defective transport observed in MeCP2- neurons. However, in order to investigate whether lithium chloride could affect the transport in MeCP2- neurons, we must first establish its effect on wild-type mice, and whether it improves BDNF transport via reduction of p-Tau.

I began by using protein immunoblotting to detect the levels of p-Tau in neurons following treatments with varying concentrations of lithium chloride. Four samples with one being the untreated control and the other three treated with 1.0, 5.0, and 25 mM of lithium chloride, respectively, for 30 minutes are analyzed by western blotting to assess their basal Tau level, and the relative decrease in p-Tau following increasing concentration of lithium chloride treatment. (Figure 3A) The results of the immunoblotting indicate greater decreases in p-Tau from the basal Tau level are correlated with higher concentrations of lithium chloride treatment, suggesting the likelihood that lithium has an overall inhibitory effect on the level of p-Tau in neurons.

For the next step of examining the effect of lithium on the axonal transport of BDNF in wild-type mice, I utilized the same protocol from the previous experiment to produce two microfluidic cultures for each wild-type mice, with one as the control and the other to be treated with lithium chloride. I also added an additional treatment stage

prior to the starvation stage on DIV 7. During the treatment stage, 5μM of lithium chloride in neurobasal-A medium is added to the treatment group, while the control group is treated with plain medium. Both groups are treated for 30 minutes before changing the media to plain neurobasal-A, and undergoing the same starvation and feeding stage as the previous experiment. After analysis, the results suggest increases in both the retrograde (+14.1%) and the anterograde (+39.2%, data not shown) transport velocities of BDNF from the control that are statistically significant (Figure 3B)

In order to further investigate whether the enhancing effects of lithium on BDNF transport are connected to the inhibition of p-Tau, I also conducted separate transport experiments with the application of corticotropin-releasing factor (CRF). A molecule whose overexpression is correlated with heightened Tau phosphorylation (ref. 62), the introduction of CRF is meant to disrupt BDNF transport by increasing the level of p-Tau, and observe whether treatment with lithium chloride could alleviate this impairment. With one microfluidic culture from each wild-type mice as the untreated control and the other treated with lithium chloride, CRF is introduced during the starvation stage to both the control and the treated groups, and the transport activities are captured through the same live imaging procedure as previously described.

Indeed, when cultures treated with only CRF are compared to control samples, the result shows significant impairments to the retrograde transport of BDNF (-39.3%).

Nevertheless, when cultures are first treated with lithium chloride before the application of CRF, marked rescues of retrograde transport velocity (+31.9%) are observed in comparison with CRF-only cultures (Figure 3B). In fact, when compared with untreated controls, lithium chloride treatment restored CRF-treated cultures to the point that there is no statistically significant difference in the retrograde transport between the two groups. This finding of the restorative capabilities of lithium on the BDNF transport of CRF-treated neurons provides support for the claim that increased p-Tau levels have a negative impact on BDNF transport, and further raises the likelihood that lithium can improve BDNF transport by reducing the level of p-Tau in neurons.

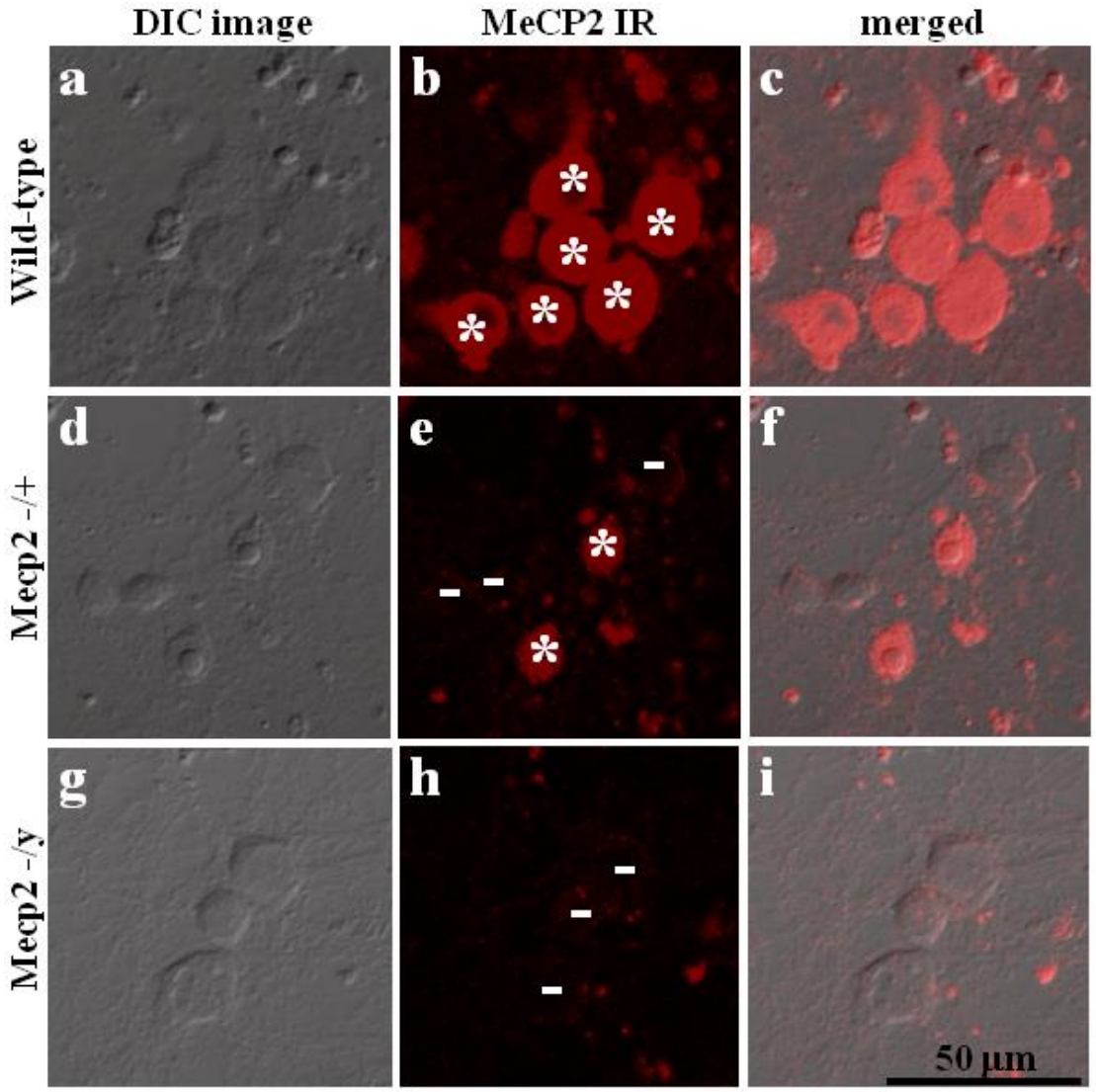

Figure 1. Phenotypic expressions of MeCP2 protein in neuronal cultures of MeCP2B litters match their respective genotypes

DIV 7 cortical neurons grew on coverslips are fixed, stained with MeCP2 antibodies, and loaded onto glass slides for examination under a confocal microscope. Differential interference contrast (DIC) images (a,d,g) and MeCP2-immunoreactivity (IR; b, e, h) from cortical neuronal cultures from wild-type (a-c), female Mecp2-mutant (d-f), and male Mecp2-mutant (g-i) mice revealed patterns of MeCP2+ (stars

in b and e) and MeCP2- (“-” in e and h) neurons that match with their respective genotypes. Scale bar = 50 um (a-i).

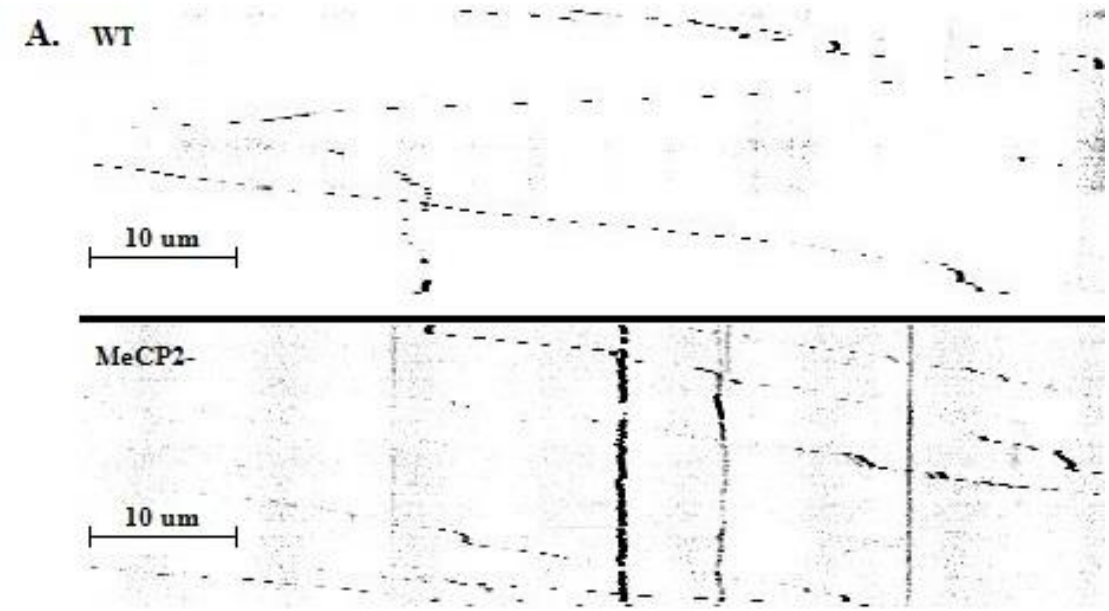

Figure 2.A: Color-inverted kymographs comparing BDNF axonal transport in wild-type versus MeCP2- neurons.

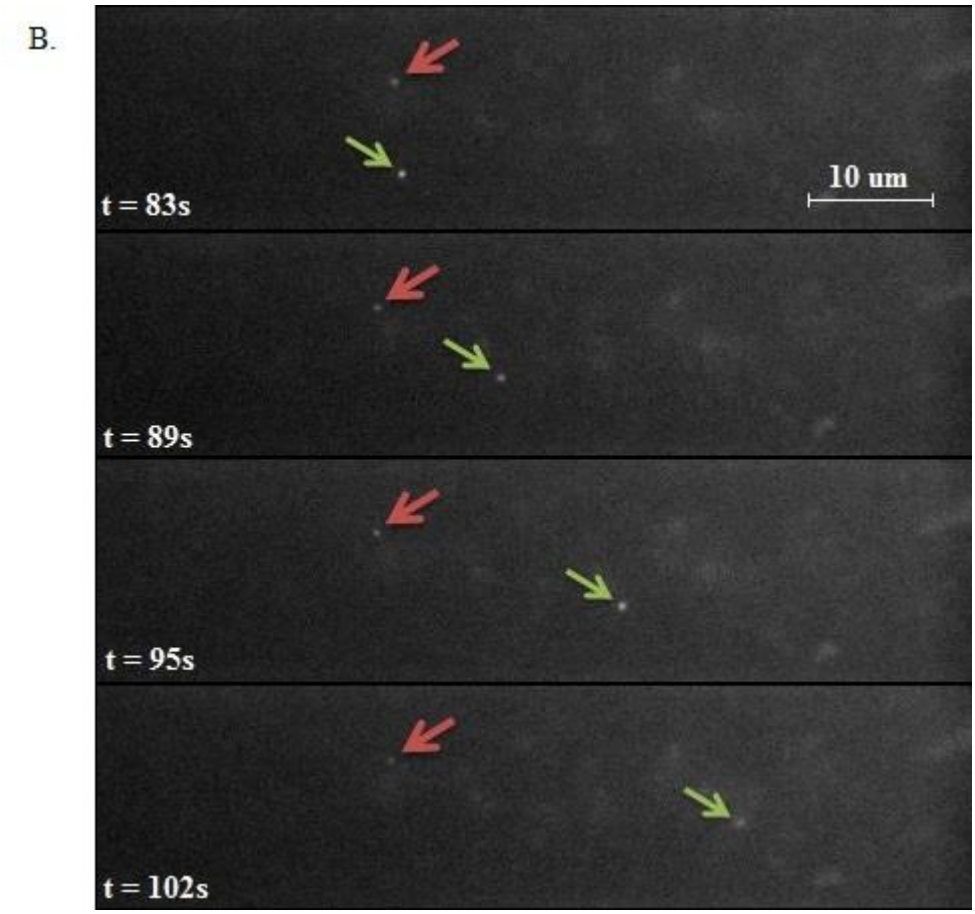

Figure 2.B: Time-lapse image series from a wild-type neuron demonstrating stationary and mobile vesicles.

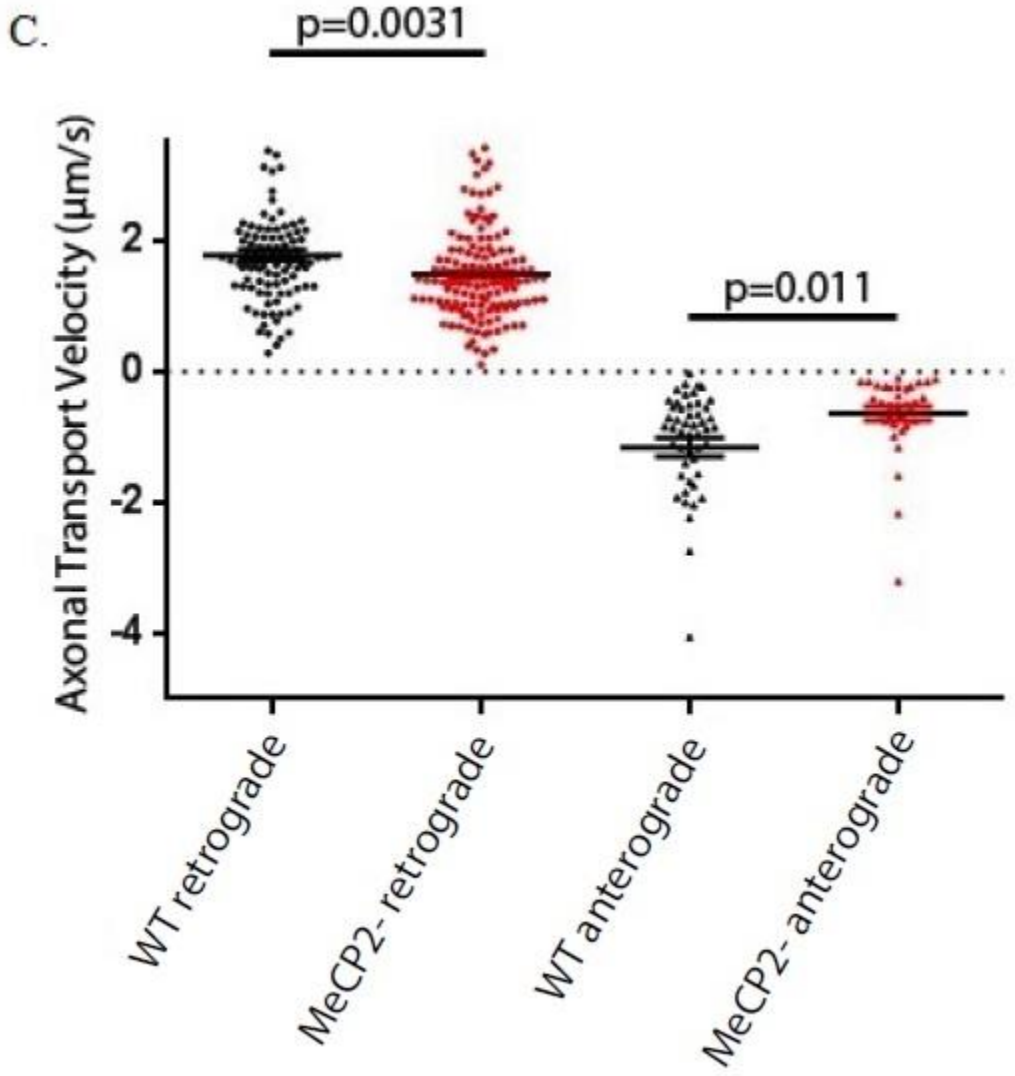

Figure 2.C: Quantitative analysis of the retrograde and anterograde transport velocities of vesicles from wild-type and MeCP2- neurons.

The number of BDNF-QD655 vesicles analyzed for each velocity group was: n=99 for wild-type retrograde; n=134 for MeCP2-/y retrograde; n=50 for wild-type anterograde; n=34 for MeCP2-/y anterograde.

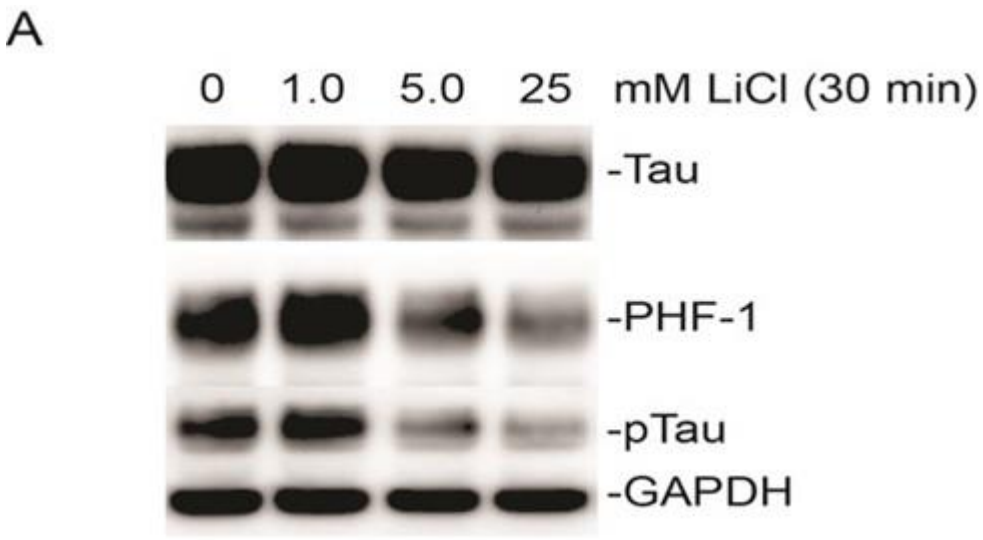

Figure 3.A: Treatments with lithium chloride have marked inhibitory effects on p-Tau and improve the axonal transport of BDNF in wild-type mice cortical neurons

Neuron samples treated with increasing levels of lithium chloride show greater decreases in p-Tau relative to the basal levels of Tau protein

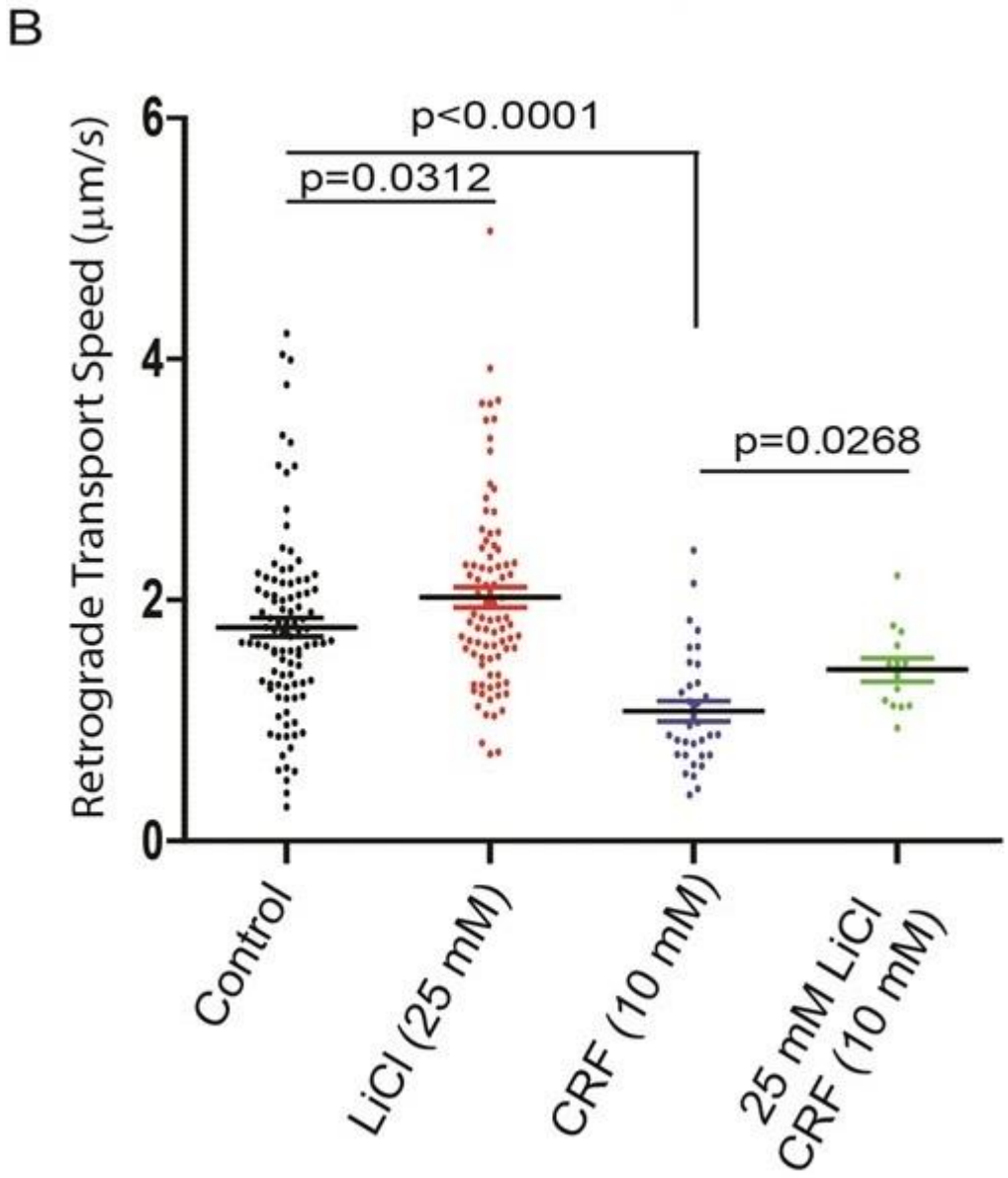

Figure 3.B: Quantitative analysis of the retrograde axonal transport velocities of vesicles containing BDNF-QD655 between cultures of the untreated control group, group treated with only lithium, group treated with only CRF, and group treated with both lithium and CRF.

The mean retrograde transport velocity ± SEM (μm/s) and the number of BDNF-QD655 vesicles analyzed for each group were: 1.773±0.07762 and n=99 for the untreated control group; 2.023±0.08580 and n=85 for the lithium only group; 1.077±0.08568 and n=33 for the CRF only group; 1.421±0.09760 and n=13 for the lithium with CRF group.

The Results chapter, in part, is currently being prepared for submission for publication of the material. Lin, Po Han. Hu, Yue. The thesis author was the primary investigator and co- author of this material.

DISCUSSION

In this project, I have first established preliminary data which confirms that phenotypic expressions of MeCP2 protein in mice from the MeCP2B model of RTT match with their respective genotypes. Then, through a combination of microfluidic cortical neuron culturing and live imaging microscopy, I have analyzed the axonal transport behaviors of BDNF in both wild-type and MeCP2-/y male mice, showing MeCP2-deficiency in neurons is correlated with marked impairments in the axonal transport of BDNF. Finally, with additional transport analysis and protein immunoblotting of neurons treated with lithium chloride, my work suggests evidence that lithium treatment enhances BDNF transport in wild-type neurons through the reduction of intracellular p-Tau level.

MeCP2-deficiency is associated with defects in the axonal transport of BDNF

While previous works have implicated symptoms and neuronal morphological changes in RTT subjects to be associated with imbalances of brain-derived neurotrphic factors in neurons, evidence suggesting how MeCP2-deficiency may contribute to these imbalances remains elusive. Fortunately, a recent study has shed some light on the potential mechanism of the relationship between MeC2-deficiency and BDNF imbalance, by showing the disruptive impact of MeCP2-silencing with siRNA on the axonal transport of BDNF in rat cortical neurons. (ref. 53) Nevertheless, direct evidence is still needed to establish that similar phenomenon occur in actual RTT models, where the MeCP2 proteins are dysfunctional due to mutations rather than

genetic silencing, in order for researchers to continue investigations in this direction to elucidate the precise mechanism of how MeCP2-deficiency influences axonal transport of BDNF. Therefore, I set out to investigate whether MeCP2 dysfunction affects neurotrophic signal trafficking in neurons from the MeCP2B mice strain, a well-established mice model of RTT (ref. 33).

Upon examining the axonal transport dynamics of BDNF in the wild-type and MeCP2-/y male neurons, I was able to observe significant reductions in both the retrograde and anterograde axonal transport of BDNF in the MeCP2-/y neurons when compared to the wild-type. However, while the differences in transport velocities are statistically significant, my results suggest a less drastic impairment in retrograde transport than the value reported in the previous publication. This may be due to differences in the backgrounds between mice and rat models, or differences between MeCP2 deficiencies caused by mutation versus siRNA silencing.

A model of BDNF imbalance caused by MeCP2-deficiency and microtubule instability

With the work from this project providing further evidence of the effect MeCP2-deficiency has on neuronal BDNF trafficking, it points toward a potential contribution of defective transport and irregular distribution of neurotrphic factors to abnormal neurodevelopment in RTT subjects. Curiously, findings of this project corroborate recent reports of increased histone deacetylase 6 (HDAC6) expressions in RTT patients correlated with tubulin and microtubule perturbations, which may play a

role in the observed impairment of BDNF transport in MeCP2-deficient neurons (ref. 63). Moreover, the effect of p-Tau on BDNF transport in RTT patients is also of interest here. In normal neuronal activities, BDNF can function as a regulator of intracellular p-Tau level, both directly through dephosphorylation of p-Tau and indirectly through inhibition of GSK-3 (ref. 61). It becomes of question then when defects of BDNF transport associated with MeCP2-deficiency has caused a reduction of BDNF present in neurons, whether this shortage of BDNF leads to hyperphosphorylation of Tau, which in turn can further induce microtubule instability and interfere with BDNF transport as observed in the CRF experiment. Furthermore, as overexpression of HDAC6 has been previously documented to cause conformation changes in heat shock protein 90 (Hsp90), leading to Tau accumulation and increases in p-Tau, the recent observation of upregulated HDAC6 in RTT subjects also raises the possibility of heightened level of p-Tau interfering with the transport of BDNF in MeCP2-deficient neurons.(ref. 64)

With the results from this project and the findings of recent publications, a model may be hypothesized to at least partially attribute common symptoms of RTT such as neurite instability and abnormal neurodevelopment to defective BDNF transports in RTT patients. The model begins with the upregulation of HDAC6 from a shortage of functional MeCP2. The overexpression of HDAC6 then leads to a reduced level of acetylated α-tubulin and conformational changes in Hsp90. The reduced level of acetylated α-tubulin would interfere with tubulin and microtubule dynamics of the axonal transport of BDNF, thereby decreasing the transport efficiency and causing

shortages of BDNF in neuron terminals. This shortage of BDNF would then cause an upregulation of p-Tau, which is further augmented by the Tau accumulation as a result of conformational change in Hsp90. The heightened level of p-Tau then causes additional instability in the microtubule assembly, impairs the BDNF transport, and leads to irregular distribution of BDNF that would result in the abnormal development of neuronal networks.

Future investigations

In order to test the hypothesized model, several topics would need to be explored with further experimentations. First, it would be logical to investigate the effect of lithium on MeCP2-deficient neurons to see whether the defective BDNF transport observed in RTT mice is at least in part p-Tau induced. This can be done with relative confidence, as the efficacy of lithium chloride treatment in reducing p-Tau level and enhancing BDNF transport even in wild-type mice has been established in this project. If the impaired BDNF transport in RTT mice is found to improve with lithium treatment, the next step would be to explore the basal Tau and p-Tau levels in MeCP2-deficient neurons to further substantiate the possibility that this impairment is correlated with heightened levels of p-Tau in RTT mice. Moreover, while it has been established in previous publications, the overexpression of HDAC6 should also be established as preliminary data through protein immunoblotting. Lastly, treatments with HDAC6 inhibitor Tubastatin A would reveal whether the compromised axonal transport of BDNF can be attributed to the overexpression of HDAC6, providing

further evidence for the hypothesized model. Through these investigations, one can also explore the potential therapeutic effects of lithium and Tubastatin A on mice models of RTT, providing further support and direction to design a treatment for RTT patients.

Table 1: Materials for mice dissection and neuronal cultures.

MATERIALS	• Sterile laminar hood
ANIMALS	• forceps
• B6.129P2(C)-MeCP2 tmi1.1Bird (Jackson Laboratory)	• scalpel
REAGENTS	• incubator
• Poly-L-lysine (R&D systems)	• Tissue culture plate 12-well (Olympus)
• Neurobasal-A media (Gibco by Life technologies)	• Petri dish 60 mm (Cytoone)
• 50X B27 neurobasal supplement (Gibco by life technologies)	• Petri dish 100 mm (Olympus)
• 100X GlutaMAX (gibco by Life technologies)	• Conic tube 15 ml (Olympus)
• Fetal bovine serum (Omega scientific, inc.)	• Conic tube 50 ml (Olympus)
• 10X HBSS (Gibco by life technologies)	• microscope
• 100X Penicillin-streptomycin (Gibco by life technologies)	• 5 ¾ glass pipette (Fisher scientific)
• 1M HEPES (Gibco by life technologies)	• Circular glass coverslip (Fisher scientific)
• 10X DNase (Roche)	• 24x30 mm glass coverslip (Corning)
• 0.25% Trypsin (Invitrogen)	**REAGENT SETUP**
• 190 proof Ethanol (Koptec)	**Dissection media (50ml) -** 5ml 10X HBSS + 1ml 1M HEPES + 500ul pen/strep + 44 ddH2O
• Alconox	
• Methanol (Fisher Scientific)	**Neuron plating media (50ml) –** 1ml 50X B27 + 500ul 100X GlutaMAX + 2.5ml FBS + 46ml NeuroB-A
• **EQUIPMENT**	
• 40 um cell strainer (Falcon)	**Neuron maintenance media (50ml) -** 1ml 50X B27 + 500ul GlutaMAX + 48.5ml NeuroB-A
• Microfluidic device (Xona)	

Cleaning glass coverslip

1. Clean glass coverslips with 30% HCl on shaker overnight

2. Recover HCl in glass container, which is reusable for two more wash procedures

3. Three 30 minutes wash with ddH2O on the shaker

4. Remove the coverslips from the glass tray into a 100 mm petri dish

5. Add 95% ethanol to the coverslips

6. Swiftly pick up one coverslip at a time using forceps and flame the ethanol to sterilize

7. Store in another clean petri dish with parafilm wrapped around to seal openings

Coat coverslip

1. For 30x40mm coverslips, place 400 ul of 1X PLL for 2 hours

    a. For circular coverslip intended for immunostaining, place the coverslips into the wells of a12-well dish, and coat each with 300 ul of 1X PLL

    b. For mass culture, coat onto the bottom of the 12-well dish with 500 ul of 1X PLL

2. Aspirate the PLL

3. Rinse with sterile autoclaved ddH2O water three times

4. Dry under laminar hood for an hour

5. Can be stored and used within 2 weeks

Chamber/coverslip assembly

1. Place PDMS chamber on top of coverslip, channel side down

2. Gently press down with pipette tip or sterile forceps until device sealed to the glass

    a. When sealing be careful with pressing near the grooves with excessive force as they can collapse and become blocked

    b. Air bubbles may become trapped in grooves if used a long time after storage

Postnatal 0 (P0) MeCP2B Mice Dissection

Mice pups are removed from vivarium on the date of birth (P0) for dissection and cultivation of cortical neurons. Ideally, the dissection should proceed within 2-3 hours after removal of the pups from vivarium to avoid potential deaths. Prior to dissection, sterilize all dissection tools in 70% EtOH for 20 minutes or longer.

1. Begin the dissection by briefly submerging one single pup in 70% EtOH.

2. Immediately sacrifice the pup on a 10 cm petri dish via decapitation with the scalpel. The process of decapitation should be one quick and smooth motion,

and done in a different dish from the one containing other live pups to avoid agitation from the smell of blood.

3. Store the tail in an eppendorf tube on ice for future genotyping.

4. Place the head on a separate shallow petri dish cover under the microscope, and pour 1 ml of dissection media over the head to prevent the brain from drying during the dissection process.

5. For each head, remove the skin with curved forceps, carefully to not damage the calvarium. One can stabilize the brain by piercing through the eye socket and hold the head in place with one hand.

6. After fully exposing the calvarium, make a cut along the midline by puncturing the midbrain region with the tip of the forceps to expose the brain.

7. Once the whole brain is visible, disconnect the olfactory bulb and remove the brain into the surrounding dissection media by scooping it out with the forceps.

8. To remove the cortices, position the brain with its ventral side up. Using the curvature of the forceps, start from the medial aspect between the ventral cortex and midbrain to cut the cortices off.

9. Strip any attached meninges from the cut cortices.

10. Transfer the cortices to a 15ml conical tube containing 2ml of dissection media, and place it on ice for dissociation after. Cortical neurons can be stored on ice for 2-4 hours before culturing.

11. Aim to complete each dissection within 6 minutes to minimize potential cell death. Sterilize the scalpel and forceps between each pup and thoroughly dry them on paper towel before proceeding to the next pup.

Cortical Neuron Dissociation and culture

1. The majority of the dissociation and culture procedures should be performed under a sterile biosafety cabinet with proper sterilization techniques when transferring materials in and out of the hood.

2. Gently wash the conical tubes containing cortices twice each with chilled dissection media.

3. Carefully aspirate the wash, and add 800 ul of dissection media to each tube.

4. Add 100ul of 10X Trypsin.

5. Incubate in a 37oC water bath for 15 minutes, gently each tube every 5 minutes.

6. Add 100ul of 10X DNase.

7. Titrate gently with a fire-polished glass pipette 7-10 times until the solution becomes cloudy with neurons.

8. Immediately add 2 ml of 37 oC pre-warmed plating media after titrating each tube to quench the Trypsin and DNase activities.

    a. Time is of essence in the titrating step to prevent cell loss while the process cannot be overly rough which would also contribute to cell deaths.

9. Allow each tube to settle for 1 minute.

10. Extract 2ml of the cell suspension, careful not to disturb the precipitated cortical parts, and pass it through a 40 um cell strainer into a 50ml conical tube.

11. Spin the tubes for 5 minutes at 1000 rpm.

12. Carefully remove the supernatant.

13. Re-suspend the cell pellets in warm plating media. The volume to suspend the pellet in will depend on the purpose of the experiment and the concentration needed. For mass culture, a concentration of 0.5-1 million cells on a 60mm petri dish is optimal. By examining the concentration of cells under a hemocytometer, proper dilution should be calculated and performed.)

14. Place appropriate amount of cell suspension into coated plates or coverslips for culture.

PDMS Microfluidic Chamber culture

1. Prepare approximately 3,000,000 cells/ml density of neuron suspension

2. Add 20ul of cell suspension into the upper left reservoir next to the channel so cells are drawn into the channel via capillary action.

3. Place chamber in humidified incubator for 10 minutes for cells to attach.

4. Add plating media to the upper left reservoir and the complementary reservoir with gradual increments on each side to avoid creation of current which would detach the cells.

5. Add media to the upper right reservoir to allow media to flow through the channel.

6. Fill all reservoirs with media, with more media on the reservoirs of the cell body side. The media surface should bulge on the neuron side. 600ul each well, 500 ul each well on non-neuron side

7. Place in humidified incubator 37C 5% CO2.

8. Change with plating media the next day, and maintenance media every other day thereon after.

9. When changing media, aspirate ½ of the media from the chamber away from the channels, and add slightly more than ½ of the ½ extracted to accommodate the evaporation

    a. Check the humidity level and media level regularly to avoid excessive evaporation and osmotic imbalance. Avoid excessive opening and closing of incubator door.

Table 2. Materials for immunostaining, genotyping, and western blot

MATERIALS	• 10% APS (Bio-Rad)
REAGENTS	• 0.5M Tris-HCl pH 6.8 (Fisher Scientific)
• Antibody for MeCP2 (Millipore)	• Tween-20 (Bio-Rad)
• Alexa Fluor 488 (Molecular Probes)	**EQUIPMENT**
• Antibody for Tau (Genscript)	• T100 Thermal Cycler (Bio-Rad)
• Ab-p-Tau (Genscript)	• Molecular Imager Gel Doc XR System (Bio-Rad)
• Ab-PHF-1 (Genscript)	• Western gel casting stand (Bio-Rad)
• Ab-GAPDH (Gentex)	• Mini Gel Caster (Bio-Rad)
• Ladder for genotyping (Lamda Biotech)	• Genotype Mini-sub Cell GT (Bio-Rad)
• AccuRuler ladder for p-Tau (Lamda Biotech)	• XCell SureLock Electrophoresis Cell (Invitrogen)
• Blot exposure liquid kit (Bio-Rad)	• Western Mini Trans-Blot Cell (Bio-Rad)
• Agarose (Fisher Scientific)	• Square transfer tray
• 2X Taq Hotstart master mix (Apex)	• Scrape bar
• Primer 9875 (Jackson Laboratory)	• Centrifuge
• Primer 9877 (Jackson Laboratory)	• Dry hot sand bath
• Primer oIMR7172 (Jackson Laboratory)	• Confocal microscope
• 6X DNA dye (Termo Scientific)	• Glass microscope slides (Fisher scientific)
• Glycerol (Invitrogen)	• PVDF Membrane (Immobilon)
• RIPA buffer (Sigma-Aldrich)	• Filter paper (VWR)
• Protease inhibitor cocktail tablet (Roche)	• Sponge
• Secondary Abs (Jackson Laboratory)	• Transfer cassette
• 3% bovine serum albumin	**REAGENT SETUP**
• Dry milk powder (Cell Signaling Technology)	**5X sample buffer:** 10% w/v SDS + 10mM β-mercaptoethanol + 20% w/v glycerol + 0.2M Tris-HCl pH 6.8 + 0.05% w/v bromophenolblue
• 4% Paraformaldehyde	
• Glucose (Sigma)	
• Triton X-100 (Sigma)	**10X TAE:** 30.2g/liter Tris + 144g/liter Glycine + 20g/liter SDS
• 5X Loading dye for protein (Bio-Rad)	
• Sodium azide (Fisher Scientific)	**Transfer buffer (1 liter):** 150ml of 100% methanol + 3.02g Tris + 14.4g glycine
• Methanol (Fisher Scientific)	
• PBS, pH 7.4 (Gibco by life technologies)	**TBST (washing buffer, 1 litre):** 2.4g Tris HCl + 0.56 Tris base + 8.8 NaCl + 990ml ddH2O + 1ml Tween-20
• 30% acrylamide (Bio-Rad)	
• 20% SDS (Bio-Rad)	
• TEMED (Bio-Rad)	**ANALYSIS TOOLS**
• 2-Mercaptoethanol (Sigma)	• ImagePad
• 1.5M Tris-HCl pH 8.8 (Fisher Scientific)	• GraphPad Prism 6

Immunostaining

1. Fix coverslips in 12-well culture dish with 4% paraformaldehyde plus 4% glucose for 30 min in a temperature and CO2 controlled incubator

2. Incubate for 5 min at room temperature with 0.1% Triton X-100 (TX-100) for permeabilization

3. Block for 45-min in blocking agent consisting of 10% donkey serum, 3% BSA, 0.1% TX-100 in PBS.

4. Incubate with primary antibodies overnight at 4 ℃,

5. Wash four times with PBS for 5 min,

6. Incubate with secondary antibodies conjugated to Alexa Fluor 488 for 1 h at room temperature.

7. Wash four additional times with PBS at room temperature

8. Dry the coverslips on kimwipes then mount onto microscope slides and seal with nail polish

Genotyping

Common forward primer 9875 20uM: 5'- AAA TTG GGT TAC ACC GCT GA -3'

MECP2 REVERSE primer 9877 20uM: 5'- CCA CCT AGC CTG CCT GTA CT -3'

WILD TYPE REVERSE primer oIMR7172 20 um: 5'- CTG TAT CCT TGG GTC AAG CTG -3'

1. Use 300ul of 50mM NaOH to digest each tail in heat bath 95C for 1 hour.

2. Neutralization with 60ul of 0.5M Tris-HCl, pH 8.

3. Spin down at maximum speed for 2 minutes to isolate DNA in supernatant.

a. The isolated DNA can be stored in 4℃.

4. Set up PCR reaction mix, including one positive control and one negative control.

Table 3. PCR mixture protocol

PCR Mix	Volume
ddH2O	8.4 ul
2X Taq Hot start master mix	10 ul
20uM Common forward primer 9875	0.2 ul
20uM MeCP2 reverse primer 9877	0.2 ul
20uM Wild-type reverse primer oIMR7172	0.2 ul
Tail-extracted DNA	1.0 ul
Final	20 ul

5. Amplify the DNA according to the following PCR program:

6. In the meanwhile, compose 30ml of 2% wt/vol of agarose solution in TAE.

7. Heat the agarose solution in microwave in short intervals, be careful to pause when boiling occurs.

Table 4: PCR program cycle

Cycle number	Denaturation	Annealing	Polymerization	Hold
1	95℃ for 15 min			
2-36	94℃ for 30 sec	65℃ for 1 min	72℃ for 1 min	
37			72℃ for 2 min	
38				10℃

8. Add 1ul of stock ethidium bromide (EtBr) to the solution.

9. When the gel is warm but not hot, pour into the mini gel caster, and allow it to solidify for 10 minutes in the cold room.

10. Add 6X DNA loading dye into the PCR-amplified samples.

11. Run 12ul of the samples in 2% agarose gel along with the controls and ladder

    a. Run the gel with 120 volts until the dye has migrated ¾ of the gel distance

12. Develop the gel with the ethidium bromide program on ImagePad

Western blot

Sample preparation

1. Rinse each well in the 12-well dish with cold PBS three times to remove any reminant of growth media
2. Add 70ul of RIPA buffer and protease inhibitor to each well

3. Using a cell scrapper, carefully remove the neurons from each well

    a. Pipette the scraped suspension to rinse the coverslip to maximize yield

4. Spin at maximum speed for 2 minute

5. Cook in 95C sand bath for 5 minutes

6. Spin again in the cold room for 10 minute with 10,000RPM

7. Add 5X loading dye

8. Load the sample into casted gel for electrophoresis

SDS PAGE-gel electrophoresis

Choose a percentage acrylamide based on the molecular weight range of proteins you wish to separate:

Table 5. Gel % for Various Protein Sizes

% Gel	M.W. Range
7	50 kDa - 500 kDa
10	20 kDa - 300 kDa
12	10 kDa - 200 kDa
15	3 kDa - 100 kDa

Table 6. Running Gel Recipe

Running gel (%)	6%	7.5%	10%	12.5%	15%
ddH2O	11.6 ml	10.6 ml	8.1 ml	6.8 ml	5.2 ml
1.5M Tris-HCl pH 8.8	5 ml	5 ml	5 ml	5 ml	5 ml
20% (w/v) SDS	100 ul	100 ul	100 ul	100 ul	100 ul
30% Acrylamide	4 ml	4.7 ml	6.7 ml	8 ml	10 ml
10% (w/v) APS	100 ul	100 ul	100 ul	100 ul	100 ul
TEMED	15 ul	15 ul	15 ul	15 ul	15 ul

Table 7. Stacking Gel Recipe

Stacking gel	4%
ddH2O	6.15 ml
0.5M Tris-HCl pH 6.8	2.5 ml
20% (w/v) SDS	50 ul
30% Acrylamide	1.33 ml
10% (w/v) APS	50 ul
TEMED	10 ul

1. Mix the gel mixture well, and add APS and TEMED last.

2. Pour 6 ml gel solution into the gel cast stand.

3. Carefully top the surface off with 100% ETOH to remove any bubbles.

4. Wait for ~30 min for gel to polymerize, meanwhile compose the stacking gel solution, add APS and TEMED only before the gel is ready to be poured.

5. Once the gel has solidified, rinse the cast with dH2O to remove the alcohol.

6. Pour the stacking gel solution into the cast, and then place the teeth on top.

7. Wait for 15 minutes for the stacking gel to polymerize.

8. After the gel has solidified, carefully remove the teeth straight up to not produce crooked wells.

9. Rinse the slots with 100% ETOH to remove any polymer remnants.

10. Store with plastic wrap and water within the wrap.

11. When ready to run the electrophoresis, add the protein samples and ladders.

12. Run the gel at 100 volts for an hour or until the dye has reached the bottom quarter of the gel.

    a. Discretion is needed to determine run time of the running stage; larger proteins require longer run time, whereas small proteins require less time as they travel faster and can be distinguished faster.

Protein transfer onto PVDF membrane

1. Prior to the end of the running stage, prepare and assemble the materials for the transfer “sandwich”

2. Wet precut pieces of membrane with 100% methanol for a few seconds then transfer to blotting buffer in a second tray. Make sure the membrane is completely submerged.

3. When the gel has finished running, carefully remove the gel from the casting stand, and cut off the upper stacking gel to be tossed.

4. Place the lower gel with proteins into the transfer assembly.

5. Dip the sponges and precut filter paper pieces in blotting buffer in a third tray.

6. Assemble the blotting sandwich as follows:

7. sponge // filter paper // gel // PVDF // filter paper // sponge

Figure 4. Blot transfer assembly

a. Make sure there are no trapped air bubbles between any of the layers

b. Assemble the sandwich on its holder so that the gel is toward the negative terminal (usually black) and the membrane is toward the positive (usually red) electrode.

c. Make sure the sponges are in good condition; if the blotting cassette is easy to close, the sponges are no good.

8. Fill the transfer apparatus with transfer buffer and apply a constant voltage of 50V for 120 min.

a. One can also transfer overnight at a low constant current (ca. 15 mA) in a cold room.

Immunostaining blot and development

1. Remove the membrane from the sandwich into a square plastic tray, and briefly rinse it with dH2O.

2. Block the blot in 5% non-fat milk in TBST for 30 min at RT.

3. Remove the milk and incubate with primary antibody either for 1-2 hr at RT or overnight in cold room on a shaker.

a. Primary Ab should be diluted with 3% milk in TBST and NaN3 for preservation.

4. Recover the primary Ab and rinse the blot briefly with dH2O.

5. Wash the blot three times with TBST for 5 minutes each.

6. Incubate with secondary Ab-conjugated to horseradish peroxidase (HRP) at dilution of 1/10,000-15,000 in TBST for 45 min to 1 hr

7. Briefly rinse the blot with dH2O.

8. Wash the blot three times with TBST for 5 minutes each.

9. On a flat bench top, flatten a piece of plastic wrap over water to create a smooth surface.

10. Create 1ml mixture of the blot exposure liquid kit for each blot.

11. Pipette 700ul of the blot exposure mixture on the plastic wrap cover for each blot.

12. Place each blot with protein side facing down over the exposure mixture for 1 minute.

    a. Ensure there are no bubbles under the blot for a clean exposure.

13. Transfer the treated blot onto the imaging system with the protein side up.

14. Aspirate some of the exposure mixture that the blot was incubated in and spray it gently over the blot for development.

15. Expose to film and develop in the imaging system with ImagePad software

    a. Select colormetric program for an image of the ladder

Table 8. Materials for BDNF Live Imaging Transport, LiCl treatment, CRF treatment

MATERIALS	• Temperature and CO2 controlled hood
REAGENTS	**REAGENT SETUP**
• Biotinylated-BDNF (provided by Dr.Chengbiao Wu, ref.65)	**LiCl solution –** 25mM
• QD-655 (Molecular Probes)	**CRF solution** – 10mM
• Neurobasal-A media	**ANALYSIS TOOLS**
• Lithium chloride (Enzo Life Sciences)	• Metamorph
• Corticotrophin-releasing factor (Robert Rissman, UCSD)	• ImageJ
• Microscope oil	• GraphPad Prism
EQUIPMENT	•
• Leica live imaging microscope	•

BDNF live imaging transport

1. Prior to DIV 7, check the distal channel of microfluidic device to confirm axons have crossed the grooves.

2. Starve neurons by first aspirate out all media, then add warmed neurobasal-A media into the top reservoirs, observe the media flowing through the channels.

3. Once fluid in the channels have been replaced by fresh media, fill up all the reservoirs.

4. Incubate for 2 hours to starve the neurons.

5. 1 hour before the starvation period ends, assemble QD-Bt-BDNF.

6. Add 5ul of 4nM purified biotinylated bdnf with 1ul of 1uM QD-655 and 14ul neurobasal-A media

7. Incubate on ice for 1 hour for conjugation.

8. Right before the starvation ends, bring the volume of the QD-Bt-BDNF up to 4 ml with warmed neurobasal-A media.

9. On the distal axon side, remove all media and add the QD-BDNF on the upper reservoir until flow through of channel media is observed

10. Add to the upper right reservoir a total of 500ul of QD-BDNF media, this will result in 250ul in each well on the non-neuron side, allowing hydrostatic pressure from the cell body side to create fluidic isolation and prevent BDNF from flowing through instead of transporting via axons.

11. Return to incubator for 2-4 hours of feeding period.

    a. Depending on cell type and models, length of feeding may differ for optimal transport observation.

    b. If too many fluorescent vesicles are observed under the microscope, reduce the feed time.

    c. If not enough vesicles are observed, increase the feed time to allow more uptake of QD-BDNF.

12. Analyze under a live-imaging Leica microscope in a temperature (37oC) and CO2 (5%) controlled environmental chamber.

    a. Using the Metamorph software, capture axonal transport with a frame capturing speed of 1 frame/second.

Lithium Chloride treatment

For LiCl treatment experiment, prior to starvation introduce the neurons with 25mM of LiCl in neuronbasal-A media for half an hour.

Lithium Chloride treatment with CRF treatment

For LiCl treatment with CRF, after the initial half an hour LiCl treatment, the starvation period should be done with neurobasal A media containing 10mM of CRF.

Making kymograph using ImageJ software

1. Open the .avi files from the captured frames in ImageJ.

2. Rotate the axons into horizontal position (Image >Rotate).

3. Crop the axons (region of interest (Image>Crop).

4. Reslice the .avi file (Image>Stacks>Reslice).

5. Make kyrographs (Image>Stacks>Z-project), select “max intensity” under “Project Type”.

6. Save the image (Kymograph).

Remove non-moving particles from time-lapse movies using ImageJ

1. Download and install a plugin for ImageJ called: "Calculator plus".

2. Restart ImageJ.

3. Open the Tiff image series.

4. Image>Stack>Z project, choose "average intensity".

5. You will create a new image, save the image as background.

6. Under Plugin, open "Calculator plus".

7. You will be asked to set i1: the image series, i2: the background image: Operation: substract.

8. You will get the cleansed image series, then from which re-do the kymograph.

Statistical analysis

The data will be exported to Excel (Microsoft, Redmond, WA) and statistical comparisons will be performed using two-tailed Student's t-tests. All results will be expressed as mean ± SEM, and P values < 0.05 will be considered to be significant.

REFERENCES

1. Rett A. [On a unusual brain atrophy syndrome in hyperammonemia in childhood]. Wien Med Wochenschr. 1966;116(37):723-6.

2. Hagberg B, Aicardi J, Dias K, Ramos O. A progressive syndrome of autism, dementia, ataxia, and loss of purposeful hand use in girls: Rett's syndrome: report of 35 cases. Ann Neurol. 1983;14(4):471-9.

3. American Psychiatric Association. (2000). Diagnostic and statistical manual of mental disorders (4th ed., text rev.). Washington, DC: Author.

4. Available at: http://www.ninds.nih.gov/disorders/rett/detail_rett.htm. Accessed October 29, 2014.

5. Davis, AS. Handbook of Pediatric Neuropsychology. Springer Publishing Company; 2010.

6. Jian L, Nagarajan L, De klerk N, et al. Predictors of seizure onset in Rett yndrome. J Pediatr. 2006;149(4):542-7.

7. Meehan RR, Lewis JD, Bird AP. Characterization of MeCP2, a vertebrate DNA binding protein with affinity for methylated DNA. Nucleic Acids Res. 1992;20(19):5085-92.

8. Nan X, Campoy FJ, Bird A. MeCP2 is a transcriptional repressor with abundant binding sites in genomic chromatin. Cell. 1997;88(4):471-81.

9. Nan X, Meehan RR, Bird A. Dissection of the methyl-CpG binding domain from the chromosomal protein MeCP2. Nucleic Acids Res. 1993;21(21):4886-92.

10. Allfrey VG, Faulkner R, Mirsky AE. ACETYLATION AND METHYLATION OF HISTONES AND THEIR POSSIBLE ROLE IN THE REGULATION OF RNA SYNTHESIS. Proc Natl Acad Sci USA. 1964;51:786-94.

11. Bird AP, Wolffe AP. Methylation-induced repression--belts, braces, and chromatin. Cell. 1999;99(5):451-4.

12. Fuks F, Hurd PJ, Wolf D, Nan X, Bird AP, Kouzarides T. The methyl-CpG-binding protein MeCP2 links DNA methylation to histone methylation. J Biol Chem. 2003;278(6):4035-40.

13. Georgel PT, Horowitz-scherer RA, Adkins N, Woodcock CL, Wade PA, Hansen JC. Chromatin compaction by human MeCP2. Assembly of novel secondary chromatin structures in the absence of DNA methylation. J Biol Chem. 2003;278(34):32181-8.

14. Bowen NJ, Palmer MB, Wade PA. Chromosomal regulation by MeCP2: structural and enzymatic considerations. Cell Mol Life Sci. 2004;61(17):2163-7.

15. Young JI, Hong EP, Castle JC, et al. Regulation of RNA splicing by the methylation-dependent transcriptional repressor methyl-CpG binding protein 2. Proc Natl Acad Sci USA. 2005;102(49):17551-8.

16. Horike S, Cai S, Miyano M, Cheng JF, Kohwi-shigematsu T. Loss of silent-chromatin looping and impaired imprinting of DLX5 in Rett syndrome. Nat Genet. 2005;37(1):31-40.

17. Yasui DH, Peddada S, Bieda MC, et al. Integrated epigenomic analyses of neuronal MeCP2 reveal a role for long-range interaction with active genes. Proc Natl Acad Sci USA. 2007;104(49):19416-21.

18. Lasalle JM, Yasui DH. Evolving role of MeCP2 in Rett syndrome and autism. Epigenomics. 2009;1(1):119-30.

19. Luikenhuis S, Giacometti E, Beard CF, Jaenisch R. Expression of MeCP2 in postmitotic neurons rescues Rett syndrome in mice. Proc Natl Acad Sci USA. 2004;101(16):6033-8.

20. Amir RE, Van den veyver IB, Wan M, Tran CQ, Francke U, Zoghbi HY. Rett syndrome is caused by mutations in X-linked MECP2, encoding methyl-CpG-binding protein 2. Nat Genet. 1999;23(2):185-8.

21. Xiang F, Buervenich S, Nicolao P, Bailey ME, Zhang Z, Anvret M. Mutation screening in Rett syndrome patients. J Med Genet. 2000;37(4):250-5.

22. Cheadle JP, Gill H, Fleming N, et al. Long-read sequence analysis of the MECP2 gene in Rett syndrome patients: correlation of disease severity with mutation type and location. Hum Mol Genet. 2000;9(7):1119-29.

23. Amir RE, Van den veyver IB, Schultz R, et al. Influence of mutation type and X chromosome inactivation on Rett syndrome phenotypes. Ann Neurol. 2000;47(5):670-9.

24. Bienvenu T, Carrié A, De roux N, et al. MECP2 mutations account for most cases of typical forms of Rett syndrome. Hum Mol Genet. 2000;9(9):1377-84.

25. Obata K, Matsuishi T, Yamashita Y, et al. Mutation analysis of the methyl-CpG binding protein 2 gene (MECP2) in patients with Rett syndrome. J Med Genet. 2000;37(8):608-10.

26. Huppke P, Laccone F, Krämer N, Engel W, Hanefeld F. Rett syndrome: analysis of MECP2 and clinical characterization of 31 patients. Hum Mol Genet. 2000;9(9):1369-75.

27. Hampson K, Woods CG, Latif F, Webb T. Mutations in the MECP2 gene in a cohort of girls with Rett syndrome. J Med Genet. 2000;37(8):610-2.

28. Wan M, Lee SS, Zhang X, et al. Rett syndrome and beyond: recurrent spontaneous and familial MECP2 mutations at CpG hotspots. Am J Hum Genet. 1999;65(6):1520-9.

29. Chahrour M, Zoghbi HY. The story of Rett syndrome: from clinic to neurobiology. Neuron. 2007;56(3):422-37.

30. Belichenko PV, Oldfors A, Hagberg B, Dahlström A. Rett syndrome: 3-D confocal microscopy of cortical pyramidal dendrites and afferents. Neuroreport. 1994;5(12):1509-13.

31. Belichenko PV, Fedorov AA, Dahlström AB. Quantitative analysis of immunofluorescence and lipofuscin distribution in human cortical areas by dual-channel confocal laser scanning microscopy. J Neurosci Methods. 1996;69(2):155-61.

32. Leontovich TA, Mukhina JK, Fedorov AA, Belichenko PV. Morphological study of the entorhinal cortex, hippocampal formation, and basal ganglia in Rett syndrome patients. Neurobiol Dis. 1999;6(2):77-91.

33. Guy J, Hendrich B, Holmes M, Martin JE, Bird A. A mouse Mecp2-null mutation causes neurological symptoms that mimic Rett syndrome. Nat Genet. 2001;27(3):322-6.

34. Belichenko NP, Belichenko PV, Li HH, Mobley WC, Francke U. Comparative study of brain morphology in Mecp2 mutant mouse models of Rett syndrome. J Comp Neurol. 2008;508(1):184-95.

35. Armstrong D, Dunn JK, Antalffy B, Trivedi R. Selective dendritic alterations in the cortex of Rett syndrome. J Neuropathol Exp Neurol. 1995;54(2):195-201.

36. Armstrong DD. The neuropathology of the Rett syndrome. Brain Dev. 1992;14 Suppl:S89-98.

37. Belichenko NP, Belichenko PV, Mobley WC. Evidence for both neuronal cell autonomous and nonautonomous effects of methyl-CpG-binding protein 2 in the cerebral cortex of female mice with Mecp2 mutation. Neurobiol Dis. 2009;34(1):71-7.

38. Belichenko PV, Wright EE, Belichenko NP, et al. Widespread changes in dendritic and axonal morphology in Mecp2-mutant mouse models of Rett syndrome: evidence for disruption of neuronal networks. J Comp Neurol. 2009;514(3):240-58.

39. Chen WG, Chang Q, Lin Y, et al. Derepression of BDNF transcription involves calcium-dependent phosphorylation of MeCP2. Science. 2003;302(5646):885-9.

40. Martinowich K, Hattori D, Wu H, et al. DNA methylation-related chromatin remodeling in activity-dependent BDNF gene regulation. Science. 2003;302(5646):890-3.

41. Chang Q, Khare G, Dani V, Nelson S, Jaenisch R. The disease progression of Mecp2 mutant mice is affected by the level of BDNF expression. Neuron. 2006;49(3):341-8.

42. Wang H, Chan SA, Ogier M, et al. Dysregulation of brain-derived neurotrophic factor expression and neurosecretory function in Mecp2 null mice. J Neurosci. 2006;26(42):10911-5.

43. Ogier M, Wang H, Hong E, Wang Q, Greenberg ME, Katz DM. Brain-derived neurotrophic factor expression and respiratory function improve after ampakine treatment in a mouse model of Rett syndrome. J Neurosci. 2007;27(40):10912-7.

44. Larimore JL, Chapleau CA, Kudo S, Theibert A, Percy AK, Pozzo-miller L. Bdnf overexpression in hippocampal neurons prevents dendritic atrophy caused by Rett-associated MECP2 mutations. Neurobiol Dis. 2009;34(2):199-211.

45. Schaevitz LR, Moriuchi JM, Nag N, Mellot TJ, Berger-sweeney J. Cognitive and social functions and growth factors in a mouse model of Rett syndrome. Physiol Behav. 2010;100(3):255-63.

46. Katz DM. Regulation of respiratory neuron development by neurotrophic and transcriptional signaling mechanisms. Respir Physiol Neurobiol. 2005;149(1-3):99-109.

47. Katz DM, Dutschmann M, Ramirez JM, Hilaire G. Breathing disorders in Rett syndrome: progressive neurochemical dysfunction in the respiratory network after birth. Respir Physiol Neurobiol. 2009;168(1-2):101-8.

48. Lioy DT, Wu WW, Bissonnette JM. Autonomic dysfunction with mutations in the gene that encodes methyl-CpG-binding protein 2: insights into Rett syndrome. Auton Neurosci. 2011;161(1-2):55-62.

49. Autry AE, Monteggia LM. Brain-derived neurotrophic factor and neuropsychiatric disorders. Pharmacol Rev. 2012;64(2):238-58.

50. Kline DD, Ogier M, Kunze DL, Katz DM. Exogenous brain-derived neurotrophic factor rescues synaptic dysfunction in Mecp2-null mice. J Neurosci. 2010;30(15):5303-10.

51. Schmid DA, Yang T, Ogier M, et al. A TrkB small molecule partial agonist rescues TrkB phosphorylation deficits and improves respiratory function in a mouse model of Rett syndrome. J Neurosci. 2012;32(5):1803-10.

52. Deogracias R, Yazdani M, Dekkers MP, et al. Fingolimod, a sphingosine-1 phosphate receptor modulator, increases BDNF levels and improves symptoms of a mouse model of Rett syndrome. Proc Natl Acad Sci USA. 2012;109(35):14230-5.

53. Roux JC, Zala D, Panayotis N, Borges-correia A, Saudou F, Villard L. Modification of Mecp2 dosage alters axonal transport through the Huntingtin/Hap1 pathway. Neurobiol Dis. 2012;45(2):786-95.

54. Park JW, Vahidi B, Taylor AM, Rhee SW, Jeon NL. Microfluidic culture platform for neuroscience research. Nat Protoc. 2006;1(4):2128-36.

55. Liu WW, Goodhouse J, Jeon NL, Enquist LW. A microfluidic chamber for analysis of neuron-to-cell spread and axonal transport of an alpha-herpesvirus. PLoS ONE. 2008;3(6):e2382.

56. Muñoz-montaño JR, Moreno FJ, Avila J, Diaz-nido J. Lithium inhibits Alzheimer's disease-like tau protein phosphorylation in neurons. FEBS Lett. 1997;411(2-3):183-8.

57. Alonso AC, Grundke-iqbal I, Iqbal K. Alzheimer's disease hyperphosphorylated tau sequesters normal tau into tangles of filaments and disassembles microtubules. Nat Med. 1996;2(7):783-7.

58. Rodríguez-martín T, Cuchillo-ibáñez I, Noble W, Nyenya F, Anderton BH, Hanger DP. Tau phosphorylation affects its axonal transport and degradation. Neurobiol Aging. 2013;34(9):2146-57.

59. Elliott E, Atlas R, Lange A, Ginzburg I. Brain-derived neurotrophic factor induces a rapid dephosphorylation of tau protein through a PI-3 Kinase signalling mechanism. Eur J Neurosci. 2005;22(5):1081-9.

60. Mai L, Jope RS, Li X. BDNF-mediated signal transduction is modulated by GSK3beta and mood stabilizing agents. J Neurochem. 2002;82(1):75-83.

61. Schindowski K, Belarbi K, Buée L. Neurotrophic factors in Alzheimer's disease: role of axonal transport. Genes Brain Behav. 2008;7 Suppl 1:43-56.

62. Campbell SN, Zheng C, Monte L, et al. Increased Tau Phosphorylation and Aggregation in Mice Overexpressing Corticotropin-Releasing Factor. J Alzheimers Dis. 2014;

63. Gold WA, Lacina TA, Cantrill LC, Christodoulou J. MeCP2 deficiency is associated with reduced levels of tubulin acetylation and can be restored using HDAC6 inhibitors. J Mol Med. 2014;

64. Cook C, Gendron TF, Scheffel K, et al. Loss of HDAC6, a novel CHIP substrate, alleviates abnormal tau accumulation. Hum Mol Genet. 2012;21(13):2936-45.

65. Cui B, Wu C, Chen L, et al. One at a time, live tracking of NGF axonal transport using quantum dots. Proc Natl Acad Sci USA. 2007;104(34):13666-71.